TDOA-Based Microwave Imaging Algorithm for Real-Time Monitoring of Microwave Ablation

Shouhei Kidera[1], Luz Maria Neira[2], Barry D. Van Veen[2], and Susan C. Hagness[2]
[1]Graduate School of Informatics and Engineering, The University of Electro-Communications, Tokyo, Japan,
kidera@uec.ac.jp
[2]Department of Electrical and Computer Engineering, University of Wisconsin-Madison, Madison, WI, USA,
susan.hagness@wisc.edu

***Abstract*—Microwave ablation (MWA) is widely recognized as a promising treatment tool for cancer. Real-time monitoring of the dimensions of the ablation zone is indispensable for ensuring an effective and safe treatment. In this paper, we propose a microwave imaging algorithm for monitoring the evolution of the ablation zone. This algorithm estimates the boundary of the ablation zone by exploiting the time difference of arrival (TDOA) between pre- and during- ablation signals received at external antennas surrounding the tissue, using the interstitial ablation antenna as the transmitter. A notable advantage of this method is that it requires few assumptions about the spatial distribution of dielectric properties of the propagation media. Also the simplicity of the signal processing, wherein the TDOA is determined from a cross-correlation calculation, allows real-time monitoring and provides noise-robust estimations. We investigate the performance of this approach using simulated array measurements obtained from FDTD simulations of MRI-derived numerical breast phantoms. The results demonstrate that our proposed method offers the potential to achieve millimeter order accuracy in estimating the boundary of the ablation zone in heterogeneous and dispersive breast tissue.**

***Index Terms*—Microwave ablation (MWA), Real-time monitoring, TDOA based boundary extraction**

I. INTRODUCTION

Microwave ablation (MWA) is a promising technique for minimally invasive treatment of primary tumors. An interstitial antenna delivers energy that heats up the cells, leading to coagulative necrosis of the malignant tumor [1]. Microwave ablation has been shown to be an effective clinical tool for treating liver tumors [2]. Although most of past research has focused on MWA of liver, there is a growing interest in MWA for treating other types of cancer, including breast cancer treatment. The success of MWA depends in part on the ability to accurately monitor the evolution of the ablation zone during the therapy procedure. Magnetic resonance imaging (MRI) [3] and ultrasound [4], [5] have been explored as MWA monitoring modalities. However, MRI has several drawbacks in terms of cost and concerns about heating MR contrast agents, and ultrasound suffers from image distortion during thermal ablation.

Microwave imaging is a promising alternative because it is portable and low cost. The data acquisition scheme can use the microwave ablation antenna as a transmitter and a number of external antennas as the receivers. Furthermore, the microwave-frequency dielectric properties of tissue are sensitive to the temperature and physiological state of the tissue. Significant changes in the microwave-frequency dielectric properties of bovine liver tissue have been observed during microwave ablation and as a function of temperature [6], [7], [8].

MWA monitoring using microwave tomographic imaging has been explored for liver tissue ablation [9] under assumptions that the dielectric properties distribution of the tissue is fairly homogeneous. Microwave tomographic techniques have also been proposed for monitoring MWA of breast tumors [10], where the tissue is much more heterogeneous. Computational cost can be reduced through the introduction of simplifying assumptions in the inverse scattering algorithm (e.g. [11]). A persisting challenge has been simultaneously achieving efficient and accurate imaging algorithms for real-time monitoring.

This paper proposes a novel real-time imaging algorithm for MWA monitoring, which exploits the time difference of arrival (TDOA) between pre- and during ablation signals and makes use of a simple propagation model to determine the boundary of the ablation zone. Our proposed algorithm comprises computationally efficient signal processing steps, namely, cross-correlation calculations to determine time delays between signals and a simple noise reduction filter (e.g. matched filter), thereby making it feasible to achieve monitoring in real-time. Another important advantage is that it requires few assumptions. It only requires an estimate of the average relative permittivity of the tissue in the vicinity of the antenna before and during ablation. We perform FDTD-based numerical simulations for two MRI-derived breast phantoms to demonstrate that our proposed method achieves accurate boundary extraction of the ablation zone, even under low SNR conditions.

II. OBSERVATION MODEL

Figure 1 shows the data acquisition configuration for our MWA monitoring strategy. The elapsed time of the ablation is denoted by T, where $T = 0$ corresponds to a time pre-ablation and $T > 0$ corresponds to a time during the ablation. The breast is constituted by skin, adipose, fibroglandular, and tumor tissues. A single transmitter (shown as a hollow black circle in Fig. 1) is inserted into the tumor, which is located within the fibrograndular tissue, and multiple receivers are

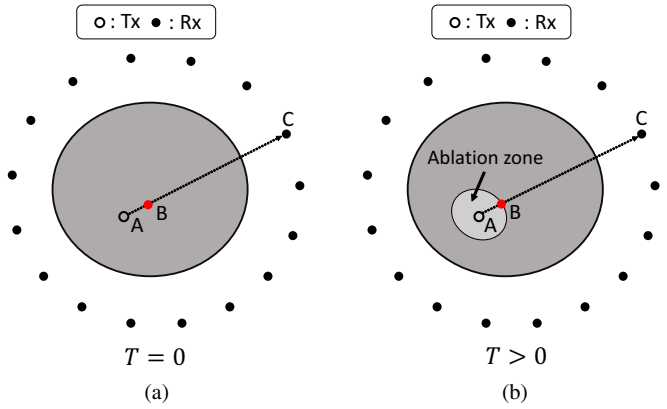

Fig. 1. Data acquisition configuration for MWA monitoring using the internal ablation antenna as the transmitter and an external array as the receivers. (a) Pre-ablation ($T = 0$). (b) During ablation ($T > 0$).

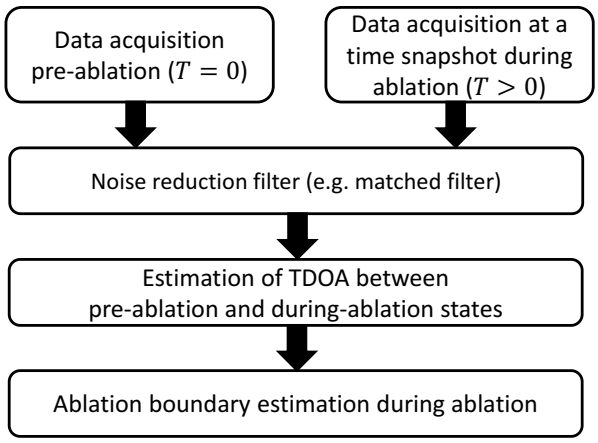

Fig. 2. Algorithm for estimating the boundary of the ablation zone at a particular moment in time during the ablation using array measurements before and during the ablation.

located surrounding the breast (shown as solid black circles in Fig. 1). The location of the source is defined as $\boldsymbol{r}_{\mathrm{A}}$, and the location of a representative receiver is defined as $\boldsymbol{r}_{\mathrm{C}}$. The received microwave signals pre-ablation (at $T = 0$) and during ablation (at the n^{th} temporal snapshot) are denoted by $s_0(\boldsymbol{r}_{\mathrm{C}}, t)$ and $s_n(\boldsymbol{r}_{\mathrm{C}}, t)$ respectively. The variable t denotes the signal recording time.

III. Ablation Boundary Extraction Algorithm

A. TDOA based boundary reconstruction

Investigations have shown that MWA leads to a steady decrease of the relative permittivity of tissues, mainly due to dehydration. The lower relative permittivity of the ablation zone leads to a significant time-delay from source to receiver, compared to the pre-ablation case. Our method exploits this principle through TDOA for extracting the ablation boundary.

Let τ_0 and τ_n be the time of arrivals (TOAs) of the pre- and during- ablation signals, respectively. The TOA can be decomposed as:

$$\tau_0 = \tau_0^{\mathrm{AB}} + \tau_0^{\mathrm{BC}} \quad (1)$$

$$\tau_n = \tau_n^{\mathrm{AB}} + \tau_n^{\mathrm{BC}}, \quad (2)$$

where τ^{AB} and τ^{BC} denote the TOAs from $\boldsymbol{r}_{\mathrm{A}}$ (source location) to $\boldsymbol{r}_{\mathrm{B}}$ (ablation boundary point), and $\boldsymbol{r}_{\mathrm{B}}$ to $\boldsymbol{r}_{\mathrm{C}}$ (receiver location), respectively, as shown in Fig. 1. We define ϵ_n as the dielectric constant of the tissue inside the ablation zone at the n^{th} snapshot, and ϵ_0 represents the dielectric constant pre-ablation. In addition, $\tau_0^{\mathrm{BC}} \simeq \tau_n^{\mathrm{BC}}$, because the dielectric properties of the tissue between B and C are invariant. Then, the TDOA between pre- and during ablation cases can be approximated as follows:

$$\Delta\tau \equiv \tau_0 - \tau_n \simeq (1 - \sqrt{\xi})\tau_0^{\mathrm{AB}}, \quad (3)$$

where $\xi = \epsilon_n/\epsilon_0$. From Eq. (3), we can approximate the distance from source to boundary point as:

$$R^{\mathrm{AB}} \equiv \|\boldsymbol{r}_{\mathrm{A}} - \boldsymbol{r}_{\mathrm{B}}\| = v_0\tau_0^{\mathrm{AB}} = v_0\frac{\Delta\tau}{1 - \sqrt{\xi}}, \quad (4)$$

where v_0 denotes the propagation velocity in the pre-ablation medium. Then, the ablation boundary point $\boldsymbol{r}_{\mathrm{B}}$ is given by:

$$\boldsymbol{r}_{\mathrm{B}} = R^{\mathrm{AB}}\,\hat{\boldsymbol{u}} + \boldsymbol{r}_{\mathrm{A}}, \quad (5)$$

where $\hat{\boldsymbol{u}}$ denotes a unit vector from $\boldsymbol{r}_{\mathrm{A}}$ to $\boldsymbol{r}_{\mathrm{C}}$.

Note that, $\Delta\tau$ can be estimated from the following cross-correlation calculation:

$$\Delta\tau = \arg\max_{\tau}[s_0(\boldsymbol{r}_{\mathrm{C}}, t) \star s_n(\boldsymbol{r}_{\mathrm{C}}, t)](\tau), \quad (6)$$

where $\star$ denotes the operator of cross-correlation. If the number of receivers is M, then M different boundary point estimates $\boldsymbol{r}_{\mathrm{B}}$ are available.

B. Procedure of the proposed method

The procedure (also shown in Fig. 2) for estimating the boundary of the ablation zone at the n^{th} temporal snapshot in time is summarized as follows:

- Step 1) Received signals are recorded at $T = 0$ (before the ablation begins) and at the n^{th} temporal snapshot during the ablation.
- Step 2) A noise reduction filter, such as matched filter, is applied to both observed signals.
- Step 3) The TDOA value ($\Delta\tau$) is determined from the peak shift of cross-correlation functions as in Eq. (6).
- Step 4) The boundary point $\boldsymbol{r}_{\mathrm{B}}$ of the ablation zone is determined using $\Delta\tau$ and the relative permittivity around the transmitter for both pre- and during ablation cases, as in Eqs. (4) and (5).

The most notable feature of this method is that it only requires the average velocity in the medium surrounding the

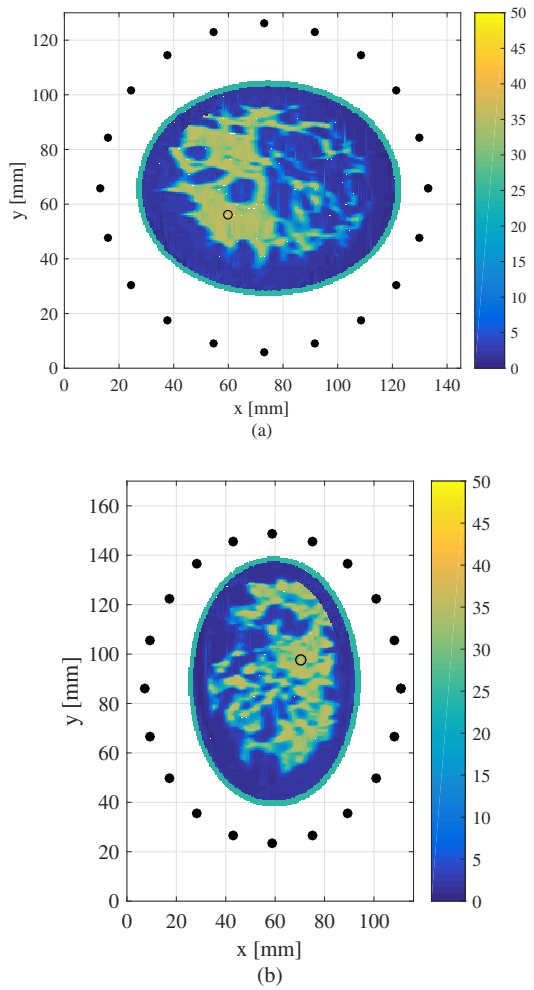

Fig. 3. Numerical breast phantoms and configuration used to evaluate the performance of the TDOA-based MWA ablation monitoring algorithm. The colorbar displays the Debye parameter, $\Delta\epsilon$. The hollow black circle denotes the location of the transmitting antenna while the solid circles denote the locations of the receiving antennas. (a) Class 3 (heterogeneously dense) breast phantom. (b) Class 4 (extremely dense) breast phantom.

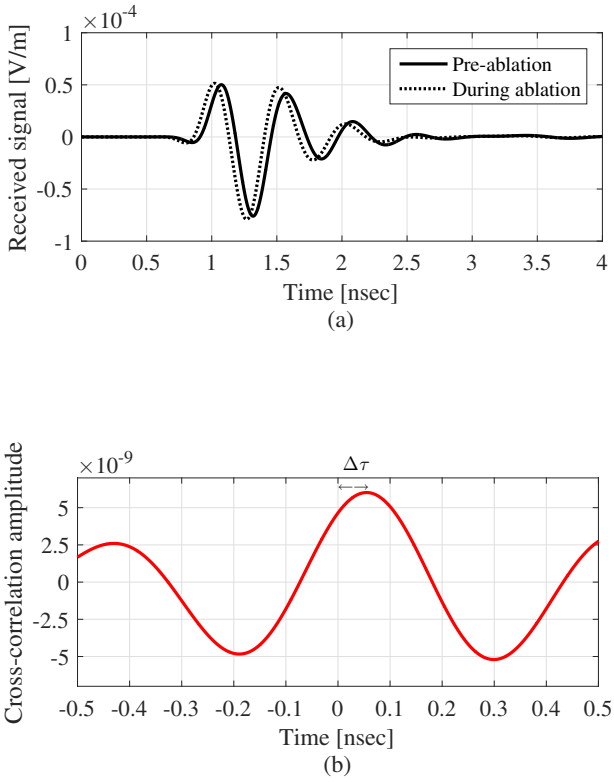

Fig. 4. (a) Electric field intensities observed at a representative receiver location ($\boldsymbol{r}_C = (133\text{mm}, 66\text{mm})$) in the Class 3 phantom. The observations are made pre-ablation and when the ablation zone is an ellipse with major axis (x-axis) of 10 mm and minor axis (y-axis) of 8 mm. (b) Cross-correlation result for the signals observed in (a). $\Delta\tau$ marks the TDOA for the representative receiver location.

source before the ablation begins, and the approximate ratio of the pre- and during-ablation dielectric constant as *a priori* knowledge. In most cases, the source will be located inside malignant tissue, whose dielectric properties are available in the literature [12]. Furthermore, the properties of ablated tissue can be determined from the growing database of dielectric properties of ablated tissue [7], [13].

IV. Two-Dimensional Numerical Simulation Examples

A. Breast phantom and simulated array measurements

We test our method using simulated measurements of two realistic breast phantoms derived from MRIs of healthy women [14]: a Class 3 "heterogeneously dense" phantom (ID number 062204), and a Class 4 "very dense" (ID number 012304) phantom. These phantoms are available online at the University of Wisconsin repository [15]. The frequency-dependent complex permittivities for skin and breast tissues in the phantoms are modeled by single-pole Debye models over the frequency range of 0.1-5 GHz, as in [10]. Figure 3 shows the map of the Debye parameter $\Delta\epsilon$ of the Class 3 and Class 4 phantoms. The transmitting source is located inside fibroglandular tissue, and it is shown as a hollow black circle in Fig. 3. We model the impact of ablation as a 40% decrease in the relative permittivity within the ablation zone (not shown in Fig. 3). This percentage drop has been observed in ablations of bovine liver tissue that has reached 99° [7]. In this case, the pre-ablation relative permittivity of the tissue surrounding the antenna was $\epsilon_0 = 47$, representing healthy fibroglandular tissue at 2.45 GHz, and ξ was equal to 0.6 in the ablation zone.

The 21 receiving antennas, shown as solid black circles in Fig. 3, are located on a ring outside breast (immersed in air) with equal spacing between them. The transmitted signal is a Gaussian modulated pulse, with 2.45 GHz as the center frequency and a 1.9 GHz frequency bandwidth. The received signals are generated using FDTD on a 0.5 mm grid. White Gaussian noise is added to each received electric field signal in

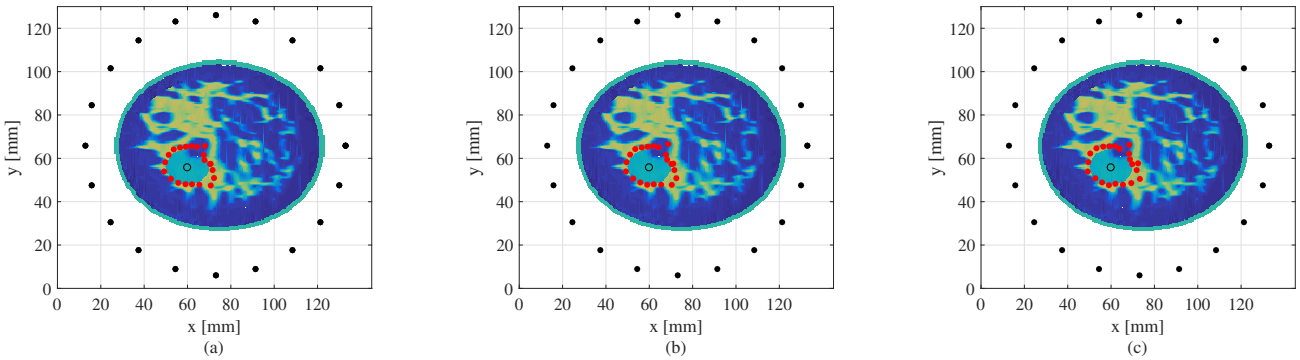

Fig. 5. Estimated boundary, shown by the red circles, of the elliptical ablation zone in the Class 3 numerical breast phantom, for different levels of SNR. (a) 20 dB. (b) 10 dB. (c) 0 dB, when the ablation zone is an ellipse with major axis (x-axis) of 10 mm and minor axis (y-axis) of 8 mm.

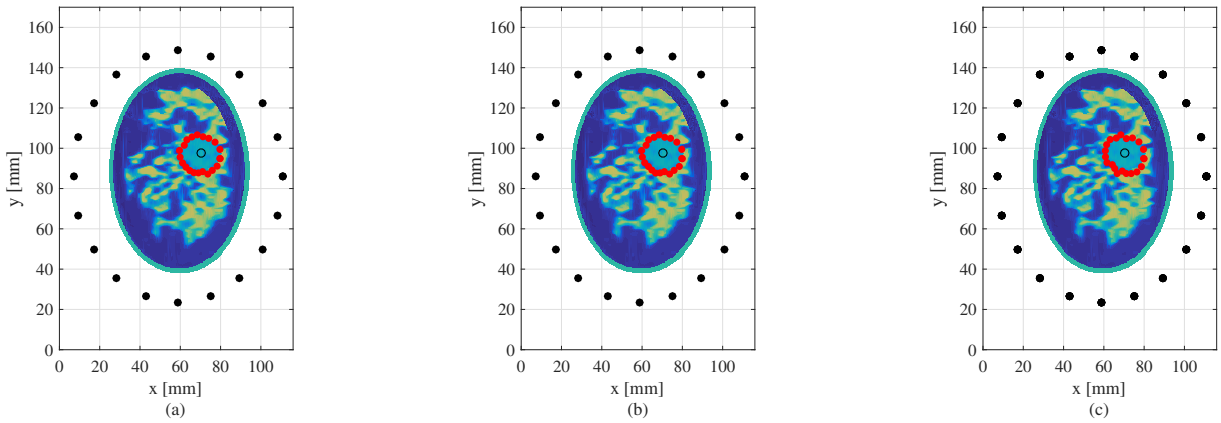

Fig. 6. Estimated boundary, shown by the red circles, of the elliptical ablation zone in the Class 4 numerical breast phantom, for different levels of SNR. (a) 20 dB. (b) 10 dB. (c) 0 dB, when the ablation zone is an ellipse with major axis (x-axis) of 10 mm and minor axis (y-axis) of 8 mm.

the time domain. The SNR is defined as the ratio between the average signal power to noise power in the time domain. We consider SNR levels of 20 dB, 10 dB, and 0 dB. A matched filter is applied to the received signals in the pre-processing step for noise reduction.

B. Results

Figure 4(a) shows as an example the time-series signals recorded at $\boldsymbol{r}_{\mathrm{C}} = (133\ \mathrm{mm}, 66\ \mathrm{mm})$ for the Class 3 phantom before and during ablation, when the ablation zone is an ellipse with major axis (x-axis) of 10 mm and minor axis (y-axis) of 8 mm; Figure 4(b) illustrates the output of the cross-correlation between the signals. Figure 4(a) shows that the representative received signal during the ablation is slightly time shifted compared to the signal pre-ablation, due to the decrease in relative permittivity of the ablation zone. It also indicates that, even in this dispersive and heterogeneous case, the waveform is not significantly distorted between pre- and during ablation times, except for the time shift, which empirically demonstrates the validity of the approximations made in the proposed method.

Figures 5 and 6 illustrate the reconstruction results in the case of the Class 3 and Class 4 phantoms for three different SNR levels, when the ablation zone is an ellipse with major axis (x-axis) of 10 mm and minor axis (y-axis) of 8 mm. The red solid circles denote the boundary points estimated by our proposed algorithm. These results demonstrate that the proposed method provides a relevant boundary reconstruction of the ablation zone, even for low levels of SNR. This noise-robust property is mainly due to the application of the noise-reduction filter (matched filter in this case). The required calculation times in any of these cases was less than 0.1 sec using an Intel Core i5 CPU 3.3 GHz, with 8 GB RAM, which validates that this method has the property of providing real-time MWA monitoring.

We define the reconstruction error as the minimum distance between each estimated boundary point and the actual boundary curve. Figure 7 shows the box plots of the estimation errors for the Class 3 and Class 4 phantoms for 100 different noise realizations for each SNR. The lower and upper bounds of the boxes denote the IQR (interquartile range) and the lower and upper whisks denote ± 2.7 standard deviation range, assuming a normal distribution. These figures demonstrate that even if the SNR is around 10 dB, the proposed method can maintain the median error within 3 mm in both cases.

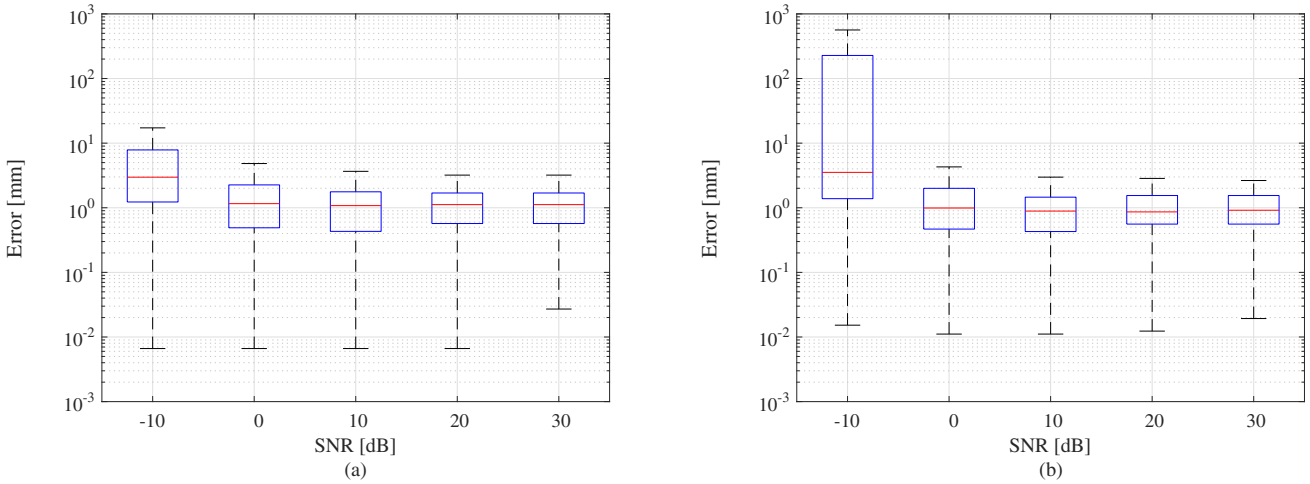

Fig. 7. Errors in ablation zone boundary estimation as a function of SNR for 100 noise instances. (a) Class 3 numerical breast phantom. (b) Class 4 numerical breast phantom.

V. Conclusion

This paper proposes a real-time ablation zone monitoring algorithm by exploiting TDOA between pre- and during ablation signals. Our proposed algorithm requires a little *a priori* knowledge, only the relative permittivity of the local treatment zone pre- and during ablation. This is a definitive advantage of our method. The numerical examples presented demonstrate that the proposed algorithm significantly contributes to real-time and accurate boundary extraction for MWA monitoring, even in situations of low SNR. Although our algorithm introduces several approximations for allowing the application of TDOA to this problem, these assumptions has been verified to be acceptable by using accurate breast models and dispersive FDTD analysis. However, it should be noted that there are some errors in the boundary estimation, even for higher SNR levels, especially for the Class 3 phantom. Such errors may be caused by the assumption of line-of-sight propagation. Further investigations will focus on extending and demonstrating this algorithm in 3D.

Acknowledgment

This work was supported by Grant-in-Aid for Young Scientists (A), Grant Number 26709030, Fostering Joint International Research, Grant Number 15KK0231 promoted by JSPS KAKENHI, and the Philip D. Reed professorship at the University of Wisconsin-Madison.

References

[1] G. Carrafiello, D. Lagana, M. Mangini, F. Fontana, G. Dionigi, L. Boni, F. Rovera, S. Cuffari and C. Fugazzola, "Microwave tumors ablation: Principles, clinical applications and review of preliminary experiences" *Int. J. Surg*. S65-9, Dec., 2008.

[2] R. C. G. Martin, C. R. Scoggins and K. M. McMasters, "Safety and efficacy of microwave ablation of hepatic tumours: a prospective review of a 5-year experience" Ann. Surg. Oncol. 17 171-8, Jan., 2010.

[3] S. Morikawa, S. Naka, H. Murayama, Y. Kurumi, T. Tani and H. A. Haque, "MRI-Guided Microwave Ablation", In T. Kahn and H. Busse (eds) Interventional Magnetic Resonance Imaging - Medical Radiology series, *Springer Berlin Heidelberg*, pp. 389-402, 2012.

[4] C. Yang, S. Wu, Y. Bai, H. Gao, "Ultrasound monitoring of temperature and coagulation change during tumor treatment with microwave ablation", J Frontiers of Biology in China, vol. 4, pp.254-259, 2009.

[5] W. Yang, M. Alexander, N. Rubert, A. Ingle, M. Lubner, T. Ziemlewicz, J. L. Hinshaw, F. T. Lee Jr, J. A. Zagzebski, T. Varghese, "Monitoring Microwave Ablation for Liver Tumors with Electrode Displacement Strain Imaging", *Proc. of 2014 IEEE International Ultrasonics Symposium (IUS)*, Sept., 2014.

[6] P. R. Stauffer, F. Rossetto, M. Prakash, D. G. Neuman and T. Lee, "Phantom and animal tissues for modeling the dielectric properties of human liver" *Int. J. Hyperth*. 19 89-101, Jan., 2003.

[7] V. Lopresto, R. Pinto, G. A Lovisolo, and M. Cavagnaro, "Changes in the dielectric properties of ex vivo bovine liver during microwave thermal ablation at 2.45 GHz", *Phys. Med. Biol*. vol. 57, pp. 2309 -2327, 2012.

[8] M. Lazebnik, M. C. Converse, J. H. Booske and S. C. Hagness, "Ultrawideband temperature-dependent dielectric properties of animal liver tissue in the microwave frequency range", *Phys. Med. Biol.* 51 1941-55, Mar., 2006.

[9] O. M. Bucci, M. Cavagnaro, L. Crocco, V. Lopresto and R. Scapaticci, "Microwave Ablation Monitoring via Microwave Tomography: a Numerical Feasibility Assessment" *Proc. of 2016 10th European Conference on Antennas and Propagation (EuCAP)*, April, 2016.

[10] L. M. Neira, B. Van Veen, S. C. Hagness, "Strategies for Monitoring Microwave Ablation of Breast Tumors using Microwave Imaging", *Proc. of 2016 IEEE AP-S Symposium*, June, 2016.

[11] M. Haynes, J. Stang, M. Moghaddam, "Real-time Microwave Imaging of Differential Temperature for Thermal Therapy Monitoring" *IEEE Trans. on Biomed. Eng.,* vol. 61, no. 6, pp.1787–1797, Jun., 2014.

[12] M. Lazebnik, D. Popovic, L. McCartney, C. B. Watkins, M. J. Lindstrom, J. Harter, S. Sewall, T. Ogilvie, A. Magliocco, T. M. Breslin, W. Temple, D. Mew, J. H. Booske, M. Okoniewski, and S. C. Hagness, "A large-scale study of the ultrawideband microwave dielectric properties of normal, benign, and malignant breast tissues obtained from cancer surgeries," *Physics in Medicine and Biology*, vol. 52, pp. 6093-6115, 2007.

[13] R. O. Mays, L. M. Neira, A. Schulman, J. Harter, L. G. Wilke, N. Behdad, and S. C. Hagness, "A pilot study of microwave ablation in ex vivo human breast tissue," USNC/URSI National Radio Science Meeting, Puerto Rico, June 2016.

[14] E. Zastrow, S. Davis, M. Lazebnik, F. Kelcz, B. Van Veen, and S. C. Hagness, "Development of anatomically realistic numerical breast phantoms with accurate dielectric properties for modeling microwave interactions with the human breast", *IEEE Trans. Biomed. Eng.*, vol. 55, pp. 2792–2800, Dec. 2008.

[15] University of Wisconsin Cross-Disciplinary Electromagnetics Laboratory (UWCEM), "Numerical breast phantom repository" [Online]. Available: http://uwcem.ece.wisc.edu, accessed on: Feb. 10, 2016.